NSRRC - Jou746 (2015)

Nanoscale

PAPER

View Article Online
View Journal | View Issue

Published on 22 April 2015. Downloaded by National Tsing Hua University on 22/06/2015 03:13:24.

CrossMark
click for updates

Cite this: *Nanoscale*, 2015, **7**, 9614

Formation of hollow silica nanospheres by reverse microemulsion†

Cheng-Han Lin,‡[a] Jen-Hsuan Chang,‡[a] Yi-Qi Yeh,[b] Si-Han Wu,[a] Yi-Hsin Liu[a] and Chung-Yuan Mou*[a]

Received 3rd March 2015,
Accepted 19th April 2015

DOI: 10.1039/c5nr01395j

www.rsc.org/nanoscale

Uniform hollow silica nanospheres (HSNs) synthesized with reverse microemulsion have great application potential as nanoreactors because enzymes or nanocatalysts can be easily encapsulated *de novo* in synthesis. Water-in-oil (w/o) reverse microemulsions comprising the polymeric surfactant polyoxyethylene (5) isooctylphenyl ether (Igepal CA-520), ammonia and water in a continuous oil phase (alkanes) coalesce into size-tunable silica nanoparticles *via* diffusion aggregation after the introduction of silica precursors. Here, we elucidate in detail the growth mechanism for silica nanoparticles *via* nucleation of ammonium-catalyzed silica oligomers from tetraethylorthosilicate (TEOS) and nanoporous aminopropyltrimethoxy silane (APTS) in the reverse microemulsion system. The formation pathway was studied *in situ* with small-angle X-ray scattering (SAXS). We find a four-stage process showing a sigmoidal growth behavior in time with a crossover from the induction period, early nucleation stage, coalescence growth and a final slowing down of growth. Various characterizations (TEM, N_2 isotherm, dynamic light scattering, zeta potential, NMR, elemental analysis) reveal the diameters, scattering length density (SLD), mesoporosity, surface potentials and chemical compositions of the HSNs. Oil phases of alkanes with different alkyl chains are systematically employed to tune the sizes of HSNs by varying oil molar volumes, co-solvent amounts or surfactant mixture ratios. Silica condensation is incomplete in the core region, with the silica source of TEOS and APTS leading to the hollow silica nanosphere after etching with warm water.

1. Introduction

Recently, hollow silica nanospheres (HSNs) have been receiving increased attention from researchers. Hollow silica nanoparticles with nanoporous shells are valuable materials for their possible functions as nanoreactors[1] in catalysis or as nanocarriers[2] in drug delivery. The nanoporous silica shell has advantages in its chemical stability, optical transparency, porous structure, and selective permeability. As a nanoreactor, it can encapsulate catalytic agents such as semiconductor nanoparticles,[3] kegging ions,[4] gold nanoparticles[5,6] or enzymes.[7,8] The porous shell could be designed as a short conduit for the reactant/product while selectively keeping poisons outside.[5,6] As a carrier in nanomedicine, its easy functionalization[1] on the external surface and the encapsulation of payloads inside can be exploited to build multifunctionality,[9,10] such as carrying drug, enzyme, contrast agent and cell recognition ligands. Its potential in both fields is rich.

In their applications, the precise synthetic control of silica nanospheres, including diameter, porosity, and encapsulation, is valuable in its future developments. Present methods of making hollow silica spheres include templating silica sol–gel synthesis with sacrificial solid nanospheres,[11] emulsion droplets,[12,13] or vesicular structures.[14–16] However, the sizes of the HSNs in most of the reports are above 200 nm in diameter, as in emulsion or vesicle templating. Such large sizes are usually not effective for biomedical applications, since cell uptake is limited. A few reports recently gave HSNs of sub-100 nm size. Hollow silica nanospheres of around 30–60 nm have been made with catanionic vesicles as template.[17] Williamson *et al.* reported the synthesis of porous hollow silica nanostructures using hydroxyapatite nanoparticle templates.[18] However, most of the reports did not show deliberate size control.

A microemulsion is a thermodynamic equilibrium system; its droplet size is thus typically uniform.[19] In principle, one can systematically control the size by changing the interfacial curvature through surfactant/co-surfactant composition or solution conditions.[20,21] With sol–gel silica condensation in the microemulsion droplets, stable solid silica nanoparticles

[a]*Center for Condensed Matter Sciences and Department of Chemistry, National Taiwan University, Taipei, Taiwan 10617, Republic of China. E-mail: cymou@ntu.edu.tw*
[b]*National Synchrotron Radiation Research Center, Hsinchu, Taiwan 30076, Republic of China*
†Electronic supplementary information (ESI) available. See DOI: 10.1039/c5nr01395j
‡These authors contributed equally.

This journal is © The Royal Society of Chemistry 2015

Published on 22 April 2015. Downloaded by National Tsing Hua University on 22/06/2015 03:13:24.

have been synthesized, in both w/o (water-in-oil) type[22–25] or o/w type microemulsion.[26] In the two types of microemulsion, the w/o type reverse microemulsion works better as template when tetraethylorthosilicate (TEOS) is used as silica source because other undesirable surfactant/silicate organizations (such as mesocellular foam) can be avoided in the oil-continuous phase.[27] In fact, w/o type microemulsion method has been used in making solid silica nanoparticles[24,25,28–30] and in the silica coating of pre-made inorganic nanoparticles.[31,32]

HSN has been synthesized by limited sol–gel condensation with w/o microemulsion, such that the incompletely condensed core can be etched away in alkaline condition.[9,10,33–35] Previously, we reported the synthesis of hollow silica nanospheres by a two-step process[3]: First, we use a Stöber-like synthesis of solid silica nanoparticle (SSN) within a reverse microemulsion (w/o) system of alkane, water, block copolymer amphiphiles, co-surfactant (hexanol), TEOS and aminopropyltrimethoxysilane (APTS). Second, an etching step in synthesizing HSN was employed to remove the core portion of silica nanoparticles. The resulting hollow silica nanospheres (HSNs) have several desirable features: (1) Cargos such as nanoparticles of gold, iron oxide[3–6] or enzyme molecules[8,36] can be easily encapsulated in the cavity of HSN. (2) The porous silica shell could function as a selective screen keeping out poisons while allowing small substrates for the catalysis.[5] The approach is especially suitable for encapsulating fragile substances such as enzymes in the water pool of the w/o microemulsion. The *de novo* enzyme encapsulation in microemulsion templating nicely solved the ship-in-bottle synthesis problem.[8,36,37] In most other approaches for making hollow metal oxides, such as in solid replacement methods,[38,39] post-synthesis loading into the cavity is limited.

For the increasingly important hollow silica nanosphere, there has been little systematic study on its formation mechanism and size control. It would be desirable to perform a systematic investigation of the reverse microemulsion templating method to understand its formation mechanism. Zhao and coworkers have systematically studied the control of the solid silica nanoparticle size by varying the organic solvents used in a w/o microemulsion alkaline synthesis.[40] Evolution of reverse microemulsion-TEOS systems in the synthesis of silica nanoparticles has also been followed.[41–44] However, there has been little mechanistic study for the hollow silica nanospheres. In this work, we study the effects of varying hydrocarbon solvents, the alcoholic co-surfactant and compositions of a mixed surfactant system on the size of the hollow silica product. We then rationalize the results by evoking the molecular model of surfactant packing for the microemulsion interface.[45]

To understand the evolution of the nanostructures in the synthesis process, we performed *in situ* SAXS measurements, a powerful technique for studying the evolution of size and density (contrast) of the nanoparticle in microemulsion.[42,44,46,47] We analyze time-resolved scattering patterns with a nanosphere model to understand their time evolution behaviors. Simulations of the patterns allow us to deduce the changes in both diameter and scattering length density. We employ a mild etching process that removes silica oligomers in the cores to produce well-defined hollow nanostructures.[48,49] The compositional changes were evaluated by elemental analysis and NMR. Combining the results of the synthesis controls of HSN sizes and *in situ* SAXS with dynamical light scattering, we finally discuss the growth of HSN in terms of a proposed formation mechanism.

2. Experimental section

Materials sources and purity are described in the ESI.† Here we give the experimental procedures for synthesis and characterizations.

2.1 Synthesis of hollow silica nanospheres (HSNs)

The hollow silica nanospheres were synthesized in a water-in-oil (w/o) reverse microemulsion system. First, 29.65 g cyclohexane, 3.26 mL CA-520 and 700 μL deionized water were mixed together and stirred at room temperature in order to generate the reverse microemulsion system. Then, 200 μL of TEOS and 50 μL of an ethanol solution of APTS were added into the mixture. The ethanolic APTS solution was prepared by adding 200 μL of APTS to 1.4 mL of absolute ethanol. Two hours later, 500 μL of ammonia hydroxide (28–30 wt%) was added to initiate the hydrolysis of TEOS and APTS. The hydrolysis and condensation process was kept at 20 °C in the synthesis of HSN and SAXS and in MAS-NMR and dynamic light scattering experiments. The as-synthesized nanospheres were separated from solution by centrifugation at 15 000 rpm for 15 min and washed with ethanol twice to remove the surfactant. Afterwards, the solid nanospheres were stirred in warm water for transforming into hollow silica nanospheres (HSNs). Again, the hollow silica nanospheres were separated from solution by centrifugation and then dried at room temperature.

2.2 Synthesis of HSNs by changing the solvent of the reverse microemulsion system

Various amounts of solvents, 29.65 g of cyclohexane, 30.29 g of *n*-hexane, 40.24 g of *n*-octane, 50.1 g of *n*-decane, and 60.0 g of *n*-dodecane were used to fix the molar ratio of the system. In order to obtain a clear solution, 2.5 mL of *n*-hexanol was added into the solutions. The rest of the work-up procedure is the same as in section 2.1.

2.3 Synthesis of HSNs by changing the ratio of CA-520 and Triton X-100

14.83 g of cyclohexane was mixed with various amounts of CA-520 (3.26, 2.45, 1.63, 0.82 and 0 mL) and Triton X-100 (0, 1.25, 2.5, 3.75, and 5 g). 0–4 mL of *n*-hexanol as co-surfactant was added into the mixture of various ratios of CA-520 to Triton X-100. 350 μL of H_2O was added into the solution to form a clear solution. 100 μL of TEOS and 25 μL of ethanolic solution of ATPS were added into the mixture, and then 250 μL of aqueous ammonia (28–30 wt%) was added into the solution

Published on 22 April 2015. Downloaded by National Tsing Hua University on 22/06/2015 03:13:24.

after 2 hours. The rest of the procedure is the same as in section 2.1.

2.4 Synthesis of HSNs by varying the volume of *n*-hexanol

The reverse microemulsion system was made with 14.83 g of cyclohexane, 5 g of Triton X-100, 350 μL of deionized water, and different volumes of *n*-hexanol (1, 3, 5, and 7 mL). It was noticed that the solution was turbid all the time, instead of clear. Then, 100 μL of TEOS and 25 μL of APTS ethanolic solution were added to the mixture under continuous stirring. After 2 hours, 250 μL of aqueous ammonia (28–30 wt%) was added to the mixture to initiate the hydrolysis of silanes, and the mixture was stirred for 36 hours at 20 °C. The as-synthesized solid silica nanospheres were isolated by adding 95% ethanol to destabilize the microemulsion system and then by centrifugation. The rest of procedure is the same as section 2.1.

2.5 Small-angle X-ray scattering (SAXS) measurements

The SAXS measurements were conducted at a BL23A SWAXS end station in the National Synchrotron Radiation Research Center (NSRRC, Taiwan) with 12 keV synchrotron X-rays (wavelength = 1.034 Å), a sample-to-detector distance of 3.8 m, and the scattering wave vector q, defined as $4\pi\lambda/\sin\theta$ with scattering angle 2θ, covering 0.005 $Å^{-1}$ to 0.2 $Å^{-1}$. The *in situ* SSN formation process was performed in a flow-cell system, as depicted in Fig. S2.† We use small-angle X-ray scattering (SAXS) technique to elucidate the morphology evolution process of silica nanoparticles. During the growth period, a solution composed of cyclohexane, CA-520, TEOS and APTS was circulated by a rotary pump between the reaction flask and a Kapton-sealed stainless cell, with a temperature-controlled cold water bath (20 °C) (Fig. S2†). Consecutive SAXS scans (Fig. 3 and S3†) with a short exposure time (30 s) were collected at various times after TEOS/APTS hydrolysis was initiated by ammonium hydroxide. Data were corrected for electronic noise, sample transmission, and detector sensitivity, then scaled to absolute intensity $I(q)$ in units of cm^{-1} *via* scattering from water. More details for SAXS data analysis can be found in ESI.†

3. Results

3.1 Synthesis and characterization

Our synthesis was conducted in a reverse microemulsion system of water-oil-surfactant with alkanes as continuous phase, water as dispersed phase, and neutral surfactant Igepal CA-520 (polyoxyethylene (5) iso-octylphenyl ether) as a surface-active agent. For the detailed mechanistic study, we focus primarily on using cyclohexane as the oil phase. Initially, the surfactant was dissolved in cyclohexane to form a clear solution. When a small amount of water (700 μL) was introduced, the solution turned turbid for a short period of time and then became clear. This indicates that a reverse microemulsion system was formed with nano-sized water droplets dispersed in the oil phase. Two silica precursors, TEOS and APTS, were initially dispersed in the oil phase and gradually hydrolyzed in the water droplet upon ammonia addition. Subsequent silica condensation, resulting in the formation of silica nanoparticles, occurred in the water phase. Representative TEM image (Fig. 1a) indicates formation of solid silica nanoparticles (SSNs) with uniform final particle sizes of 30 ± 3 nm. The solid nanoparticles were transformed to hollow silica nanospheres (HSNs) by washing with a warm ethanol–water solution (40–50 °C). During the washing, silicate oligomers (in the core) and some of the amphiphiles (on the shell) are extracted. There is little size reduction or shape deformation in the etching process as evidenced by the TEM images of SSNs and HSNs (Fig. 1c and d). For the cyclohexane system, the final dried HSNs show an average diameter of 29 nm and a shell thickness of around 5 nm (Fig. 1b).

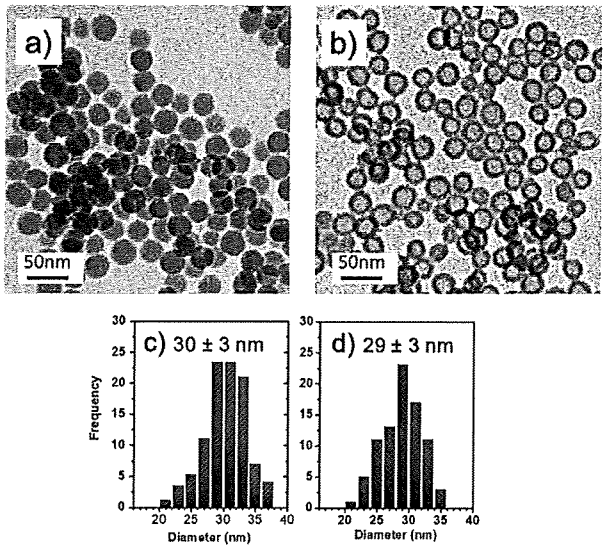

Fig. 1 Representative TEM images and size distribution analysis of the un-etched solid silica nanoparticles (SSNs) (a, c) and hollow silica nanospheres (HSNs) (b, d).

The N_2 adsorption–desorption isotherm (Fig. 2) shows a peculiar texture (the hysteresis loop), different from the amorphous silica of nanoparticles obtained by Stöber synthesis.[50] This is due to the nanopores on the shells of HSNs. The surface area and pore volume of the calcined HSNs are 359.14 $m^2\ g^{-1}$ and 1.09 $cm^3\ g^{-1}$, which are not greatly larger than those of as-washed HSNs (170.74 $m^2\ g^{-1}$ and 0.72 $cm^3\ g^{-1}$, Table 1). The large surface areas are partly attributed to the mesopores on the shells that were initially occupied by CA-520 but later removed by extraction and further by calcination. The micropores (less than 1 nm) in HSN and calcined HSN are responsible for a substantial fraction of the total area. In SSN, the pores are completely microporous in nature. These micropores (less than 1 nm) are the result of the stacking of very small nanoparticles, which are also present in Stöber silica. After washing to create the hollow voids, some pores are

 This journal is © The Royal Society of Chemistry 2015

Published on 22 April 2015. Downloaded by National Tsing Hua University on 22/06/2015 03:13:24.

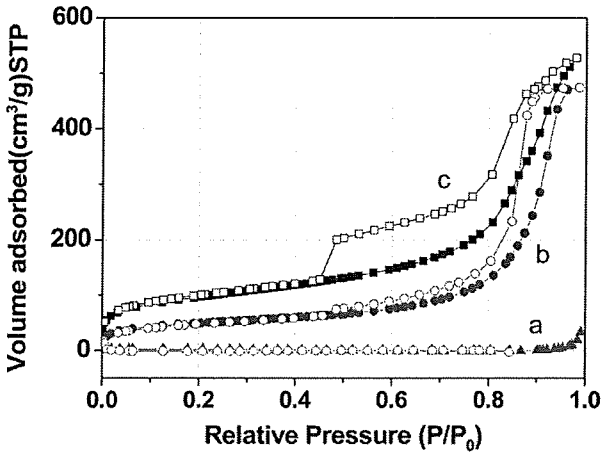

Fig. 2 N_2 adsorption–desorption isotherms of (a) SSN (red), (b) as-prepared HSNs after warm-solution washing (blue) and (c) HSNs after calcination at 560 °C (black).

Table 1 Textural properties of SSN, HSN and calcined HSN determined by N_2 adsorption isotherms

	BET surface area ($m^2\ g^{-1}$)	Pore volume ($cm^3\ g^{-1}$)	Micropore surface area (t-plot, $m^2\ g^{-1}$)
SSN	6.09	0.05	6.09
HSN	170.74	0.72	53.66
Calcined HSN	359.14	1.09	206.35

already created in extraction to connect the outer and inner voids, and thus there is no significant difference in pore volume between as-washed and calcined HSNs. After calcination, the hysteresis loops in the isotherm increases and shifts to lower-pressure regimes (Fig. 2b, $0.45 < p < 0.8$), resulting in smaller pores on the HSN particles. In comparison, the surface area and pore volume for unwashed SSNs are much smaller (Table 1). Zeta potential measurements were measured on the as-etched HSNs in a titration pH range between 3 and 10 (Fig. S1†) The isoelectric point of the HSNs is determined at pH = 5.2, which is significantly higher than those of amorphous silica (around pH = 2–3). The higher isoelectric point is due to the functionalized amine group in the HSNs. Below the isoelectric point (pH < 5), HSNs become positively charged due to protonation of amines in APTS. Above the isoelectric point (pH > 6), the HSNs are negatively charged due to deprotonation of surface silanol groups.

3.2 Time evolution by SAXS

Initial examination of the SAXS profile in Fig. 3a indicates a growth of a polydisperse distribution of nanospherical domains as time increases. Except for the two initial time data which can be fitted by unimodal size distribution of nanospheres, all the SAXS data for the rest of the time were fitted by bimodal distribution of various SLD sizes. Four selected fittings of SAXS profiles are shown in Fig. 3b–e. At initial time, the low q part of the SAXS spectra did not indicate any particle larger than 15 nm. Thus, we fit the SAXS spectra with the unimodal distribution of spheres of diameters less than 15 nm. Compared to the SAXS of collected and dried SSNs (Fig. 3e), the lesser oscillation at intermediate q (~0.02 A^{-1}) in Fig. 3e indicates there is population of small nanostructures around ~10 nm coexisting with the silica nanospheres in solution, thus smearing out the SAXS oscillations.

Before silica condensation, the microemulsion shows a water droplet size of 8 nm. From the IGOR fitting analysis, nanoparticles with increasing SLD values and growing sizes were identified after the addition of ammonia solution. The

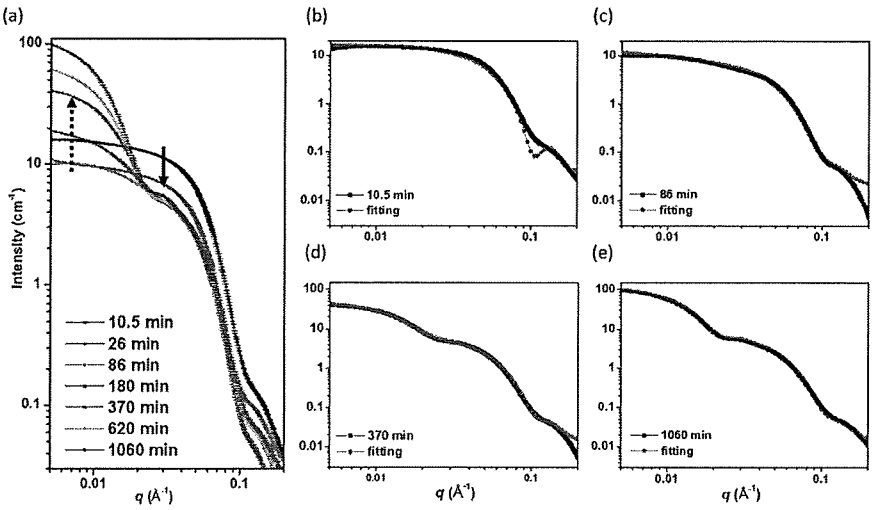

Fig. 3 (a) All SAXS experimental (dot-curve) and selected fitting results (red dot-curve) from bimodal spheres in the Schulz size distribution function for SSN growth reaction after (b) 10.5 min, (c) 86 min, (d) 370 min, and (e) 1060 min.

Published on 22 April 2015. Downloaded by National Tsing Hua University on 22/06/2015 03:13:24.

nanoparticles with larger SLD values can be directly evidenced in TEM images (Fig. S4†), which indicate that the growth of silica nanoparticles evolve from a size similar to the microemulsion droplet (7–8 nm). Within the first hour of initiation, a quick reduction in SAXS intensities indicates a consumption of the microemulsion droplet population and a small growth of particle sizes (~10 nm, Fig. 4b). At about the same time, the fitted SLD (Fig. 4a) shows a rapid increase with time, suggesting a rapid hydrolysis of TEOS and APTS and nucleation within the w/o droplet. We also see a very large fluctuation in nanoparticle size at about 100 min, which is characteristic of a period of rapid nucleation burst.[51] After 100 min, the total scattering intensity at low q gradually increased, giving a continuous increase in silica nanoparticle size, while its SLD remains roughly constant until 600 min. In this period, the continuous growth of silica nanoparticle size is driven by the coalescence of hydrolyzed TEOS and APTS inside the microemulsion droplet. The medium-q scattering profile ($0.006 < q < 0.1$) is mainly due to increasing sizes and SLD values of the growing nanoparticles, whereas the high-q scattering profile ($q > 0.1$) yields sizes and SLD values for those of the initial microemulsion droplets. The SAXS and fitting results from the medium- and high-q regimes can provide us a picture of the evolution of diameters and SLD values as well as of aggregative behaviors during the growth process. We observed a bi-modal distribution of spherical nanoparticles. The smaller ones of 8 nm size with low and unchanging SLD are the water droplets in microemulsion. Apparently, those are the un-nucleated droplets with mainly water inside. The large growing spheres are the sink sites for coagulation driven by silica condensation. The coagulation behaviors of the nanoparticles suggest a coalescence pathway for the final SSNs. Diameter distributions and the SLD values can be derived from polydispersity (ρ) and its fitted diameter (d).

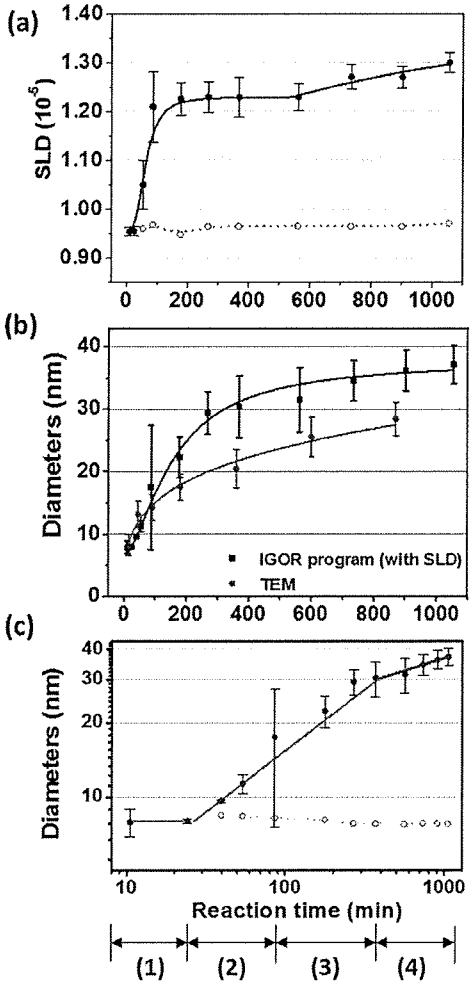

Fig. 4 (a) SLD calculations and (b) diameters of solid silica nanoparticles (●) and reverse microemulsion (○) *via* bimodal spheres in the Schulz size distribution function with polydispersity parameters for diameter uncertainty. (c) Stages of the size evolution for SSN growth as denoted under *X*-axis: (1) induction period, (2) nucleation burst, (3) growth by diffusion-coalescence, (4) slowdown of growth stage.

We plotted the growth parameters (SLD and diameter) of the SSNs with individual variance bars as shown in Fig. 4a and b. In the earliest stage (<30 min), the variance for the diameters and SLD values were relatively small, with a nearly constant diameter size (~8 nm) and SLD ($9.5–9.7 \times 10^{-6}$ Å^{-2}) for the microemulsion comprising only water. After 1.5 h (90 min), SAXS profiles suggest increased polydispersities (~0.3 in Fig. 4a) that coincide with an observation of wide diameter distributions in TEM analysis (Fig. S3†). This phenomenon suggests that the initial nucleation of SSNs results in large diameter fluctuations with higher polydispersity. In the next few hours, the SSNs grew to be larger than 30 nm, and SLD values increased to 1.23×10^{-5}, whereas the SLD values for pure H_2O and silica are known to be 9.46×10^{-6} and 1.8×10^{-5} Å^{-2}, respectively.[52] The SLD contrasts between H_2O and silica suggest that SSNs are low-density soft silica matrix comprising of mainly H_2O, ethanol and some partially condensed silica from which less condensed silicates may be removed by washing with warm water. In the period 1.5 to 10 hours (metastable zone), the SLD values reached the first plateau stages by absorbing hydrolyzed polymeric silica inside the microemulsion water droplets. In the next 10–18 hours, the silica nanoparticles matured with a small increase in SLD. Apparently, water was further consumed in silica condensation, and one sees a further small increase in SLD. The final SLD value (1.3×10^{-5} Å^{-2}) never reaches the high value for pure silica (1.8×10^{-5} Å^{-2}). Thus, the final SSNs collected by centrifugation still contain a substantial amount of uncondensed silanol and are thus removable by washing. In Fig. 4b, we also plotted the final size of collected SSNs as measured by TEM (red curve). Since the SSNs are collected after precipitation, centrifuge and drying, excess water and alcohols in the droplet pools have been removed. Thus, the size of SSNs determined by TEM is expected to be smaller than the size of water droplets in the reverse microemulsion.

In order to better understand the growth mechanism of the silica nanoparticle in solution, we re-plotted the time evolution

 This journal is © The Royal Society of Chemistry 2015

Published on 22 April 2015. Downloaded by National Tsing Hua University on 22/06/2015 03:13:24.

of its diameter in a log–log graph as shown in Fig. 4c. One can clearly see that the evolution can be divided into stages. We discuss the growth mechanism in greater detail based on this plot in the discussion section, after the rest of the experimental data in this section are presented.

3.3 Etching to form hollow nanospheres

After the nanoparticles (SSNs) were made, they were etched in warm water to make hollow nanospheres (HSNs) with interior hollow cavity and nanoporous silica shell. Fig. 5 shows the time evolution of the etching process. The initial SSN was quite uniform in size. Initial etching at 10 min of washing shows many isolated, small voids inside the SSNs. At 20 min, we obtained hollow center voids with some residue silica inside (Fig. 5c). Finally, at 40 min, well-etched HSNs were obtained showing the same size as the original SSNs. Elemental analysis and ^{29}Si NMR can monitor TEOS and APTS condensation and etching-release degrees during the process. The ~5 nm thick shells in HSNs contain double the amounts of nitrogen element (from APTS) as that in the SSNs, while the supernatant solution from the etching process contains only small amounts of nitrogen (Table S1†). According to the C, H, N elemental analysis (Table S1†) and mass-transfer calculations of APTS, TEOS, CA-520 and SiO_2 (Table S2†), the HSN shells receive 35.8% of TEOS derivatives and 76.1% of APTS derivatives from the SSNs prior to the etching process. The washed-out content was mainly water and TEOS derivatives (64.2%), with a minor quantity of APTS (23.9%). To further investigate the siloxane species in as-synthesized silica, solid-state ^{29}Si NMR spectroscopy was employed to evaluate the degrees of condensation before and after the etching procedure. In Fig. 6, one observes a significant reduction of Qx species, while the T species due to APTS remain at about the same level (Fig. 5a, red to blue curves). This confirms the fact that TEOS derivatives were the dominant leached species from HSN cores. After deconvolution of Gaussian profiles, slightly increasing Q^3 and Q^4 and decreasing Q^2 intensities (Fig. 6 and Table S3†) indicate that condensation continued to occur during the etching process.

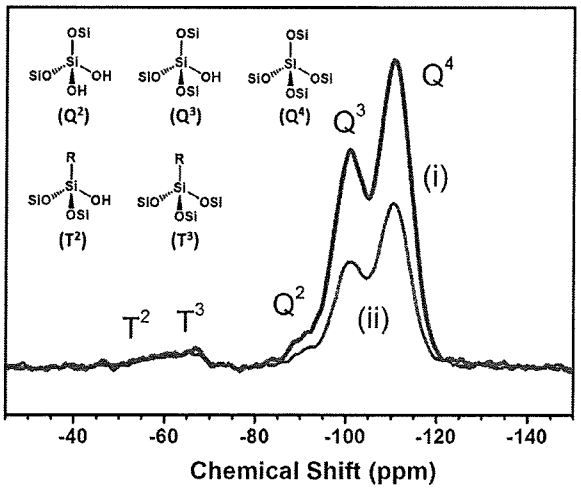

Fig. 6 ^{29}Si solid-state NMR spectra of SSNs (i, red curve) and HSNs (ii, blue curve).

Also in the etching process, the ethanol washing step removes the surfactant CA-520. It not only removed the surfactants on the external surface, but also created some pores by removing the pore-templating surfactant. In the next warm-

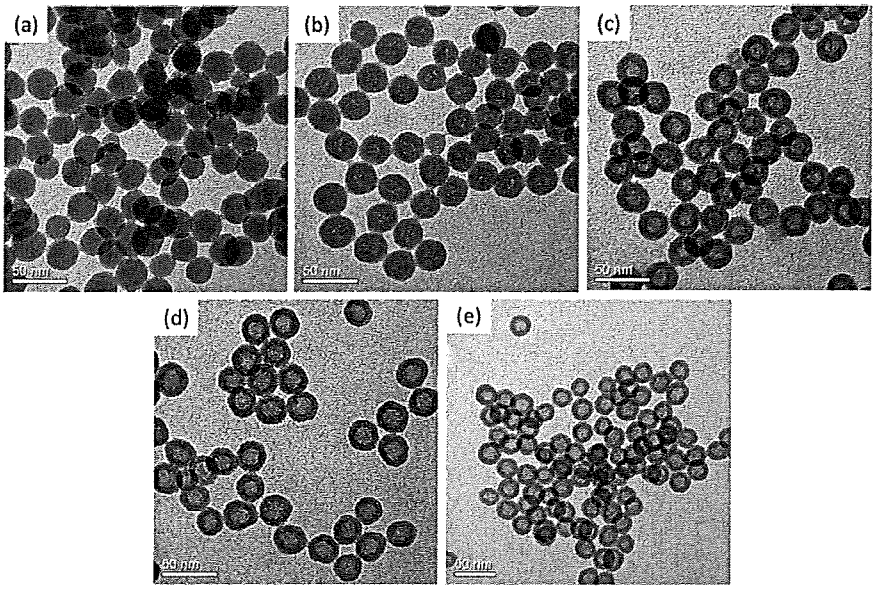

Fig. 5 The etching process of HSN at (a) 0 min, (b) 10 min, (c) 20 min, (d) 30 min and (e) 40 min.

Published on 22 April 2015. Downloaded by National Tsing Hua University on 22/06/2015 03:13:24.

water washing step, the uncondensed species inside the SSNs (mainly from TEOS) were leached out through the pores on the shell. In summary, the etching process in warm solution successively releases mainly TEOS and minor APTS derivatives into the solution. The synthesis of HSNs critically depends on incorporating APTS, which leads to the partial condensation and removal of TEOS in the facile washing process.[9,10]

3.4 Growth mechanism

Here we propose a mechanism for the formation of uniform hollow silica nanospheres in the w/o microemulsion. The reverse microemulsion serves as a soft container to initiate the nucleation and growth of silica nanoparticles, in alkaline condition, that can be systematically transformed into hollow nanospheres (HSNs), as illustrated in Scheme 1. The initial droplets (~8 nm as observed in SAXS spectra) in the reverse microemulsion are mainly water. The hydrophobic silica source TEOS dissolves in the oil phase of cyclohexane. The amphiphilic CA-520 and APTS reside mostly at the oil/water interface of the droplet. After NH_4OH was introduced into the reverse microemulsion, TEOS and APTS were catalytically hydrolyzed to form silanol groups (Si–O^- or Si–OH), moved into the water droplet in the microemulsion and condensed into polymeric species.[53] After inter-droplet collision/exchange, the polysilicate species could initiate the nucleation of silica nanoparticles. Further growth of the surfactant-stabilized nuclei then occurs through inter-droplet coalescence. Initially in the first 100 min, the sizes and SLD greatly fluctuated due to coexistence of different nanoparticle diameters, as they were just nucleated. However, after that, nucleation was quenched; subsequent growth process became size-focusing, as indicated by the reduced size variance in Fig. 4c.

3.5 The effect of alkane chain length

With the growth mechanism understood, we varied the oil phases in the reverse microemulsion systems, which may impact the sizes of HSNs. Using alkanes of different chain lengths, *e.g.* *n*-hexane, *n*-octane, *n*-decane, and *n*-dodecane as the continuous oil phase, we can create reverse microemulsion systems with different initial sizes. In all samples, a fixed amount of co-surfactant (*n*-hexanol, 2500 μL) was added to stabilize the microemulsion in these oil/surfactant systems. All experiments were also conducted with the same molar ratio of the oil component to the surfactant (CA-520). After the same growth process at 20 °C for 36 hours, the size of HSNs (from TEM images) synthesized from different oils are shown in Fig. 7a–e. The average diameters of HSNs for products from *n*-hexane, *n*-octane, *n*-decane, and *n*-dodecane were determined as 42 ± 4 nm, 51 ± 6 nm, 60 ± 5 nm, and 71 ± 7 nm (Table S4†). All the HSNs are very uniform in size, with around 10% size variance. Roughly speaking, a linear correlation between the HSN diameters and the solvent molar volume was found (Fig. 7e). The HSN diameters became larger as oil chain-length was increased. We also employed dynamic light scattering (DLS) to measure the microemulsion droplet sizes before the introduction of TEOS or APTS. The size distributions of hydrodynamic diameters are shown in Fig. S5.† The w/o microemulsion system in *n*-hexane has shown the smallest droplet size among all oil phases. The hydrodynamic diameters of the w/o microemulsion droplets are positively correlated to the chain lengths of alkane. Previously, Zhao and coworkers reported a synthesis of silica nanoparticles using Triton X-100, with a similar trend in tuning sizes using these alkanes.[40] Compared to Stöber silica, the size distributions here are broader, which is due to the presence of APTS in our synthesis.[36] However, compared to silica hollow spheres reported in literature (except by hard templating), our HSNs are relatively uniform (less than 15% dispersity).

3.6 Effect of co-surfactant

It is known that the particle sizes synthesized in a microemulsion system are governed by the amount of cosurfactant besides the bulkiness of the oil molecule.[20] So, we investigate the effect of the co-surfactant (*n*-hexanol) on the diameters in HSN synthesis for the cyclohexane system. Here, we use the surfactant Triton X-100 instead of CA-520. Triton X-100 has longer hydrophilic groups than CA-520, while their hydrophobic groups are the same. To form a stable microemulsion, a co-surfactant of more hydrophobic balance would be needed. The microemulsion system was composed of cyclohexane, water, Triton X-100, and *n*-hexanol. Without introducing *n*-hexanol in the system, the microemulsion could not be

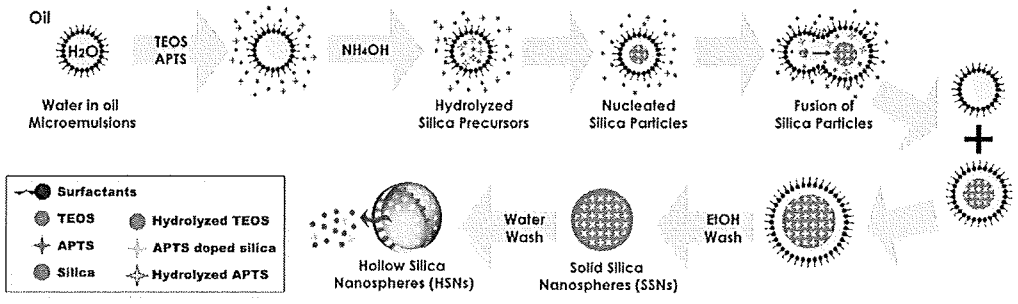

Scheme 1 The nucleation and growth mechanism of silica nanoparticles and nanospheres.

 This journal is © The Royal Society of Chemistry 2015

Published on 22 April 2015. Downloaded by National Tsing Hua University on 22/06/2015 03:13:24.

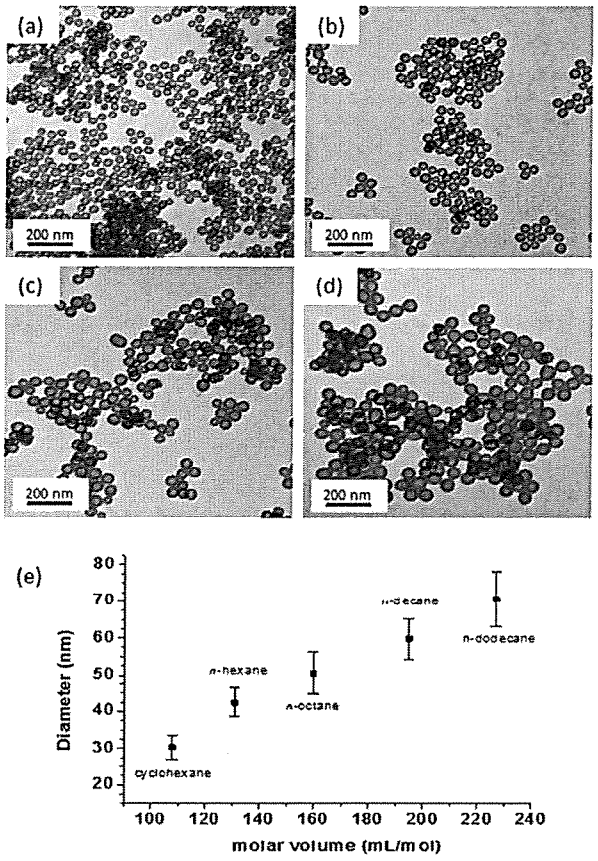

Fig. 7 Representative TEM images for HSNs synthesized in various alkyl-chain solvent systems: (a) *n*-hexane, (b) *n*-octane, (c) *n*-decane, (d) *n*-dodecane. The size distributions and their correlations to the solvent molar volumes are plotted in (e).

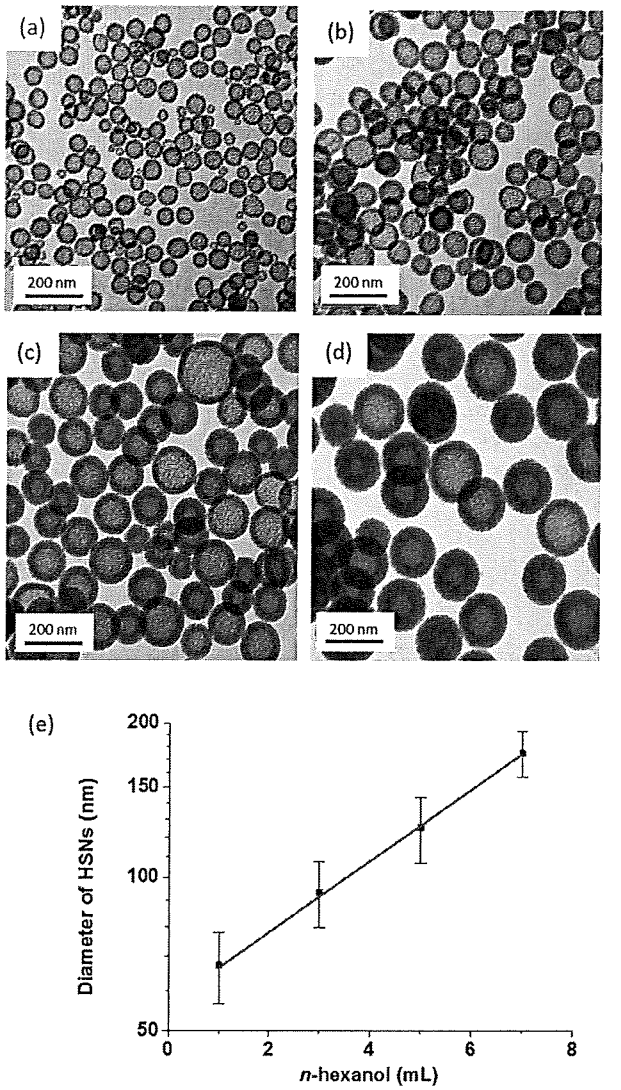

Fig. 8 TEM images and size distribution of HSNs synthesized in the cyclohexane system with different volumes of *n*-hexanol: (a) 1 mL, (b) 3 mL, (c) 5 mL, (d) 7 mL. (e) A relationship between the different volumes of *n*-hexanol added and the corresponding diameters (in log scale) of the HSNs.

formed because the hydrophilic PEO group is too short, and water and oil phases became immiscible. A co-surfactant, such as hexanol, is necessary to form the microemulsion. After the same synthesis and etching process, the images and size distributions of HSNs are compared in Fig. 8. Representative TEM images indicate that the nanosphere sizes and shell thicknesses increased with the amounts of *n*-hexanol added. A linear correlation of the final HSN diameters (60–170 nm in log scale) to the volumes of added *n*-hexanol was observed in Fig. 8e and S6b.† However, this diameter trend of *n*-hexanol-added volume gives an opposite correlation to their initial microemulsion water droplet sizes. For example, adding 7 mL of *n*-hexanol into Triton X-100 system gives the smallest-sized reverse micellar size in microemulsion, but develops the largest HSNs (175 nm, Fig. S6†). We note here that the co-surfactant *n*-hexanol behaves like a surfactant, in that increasing the co-surfactant/surfactant would create more interfaces thus forming more smaller-sized droplets. The final increase in diameter of the resulting HSNs with respect to the amount of hexanol is explained in section 4.2. To sum up, using *n*-hexanol as a co-surfactant to control the size of HSNs is a simple and effective method. The size of HSNs can be tuned from 60 nm to 170 nm as the added amount of *n*-hexanol is increased.

3.7 Effect of surfactant mixture

Finally, we examine the effect of mixing two surfactants. It has been observed that Triton X-100 can lead to HSNs with diameters larger than those made from CA-520. Therefore, one expects that mixing these two surfactants may interpolate the diameters between HSNs made with a single surfactant. As shown in the TEM images in Fig. 9, the size of the HSNs increased as the relative molar ratio of Triton X-100 to CA-520 was increased. In addition, we observed significantly increased

Published on 22 April 2015. Downloaded by National Tsing Hua University on 22/06/2015 03:13:24.

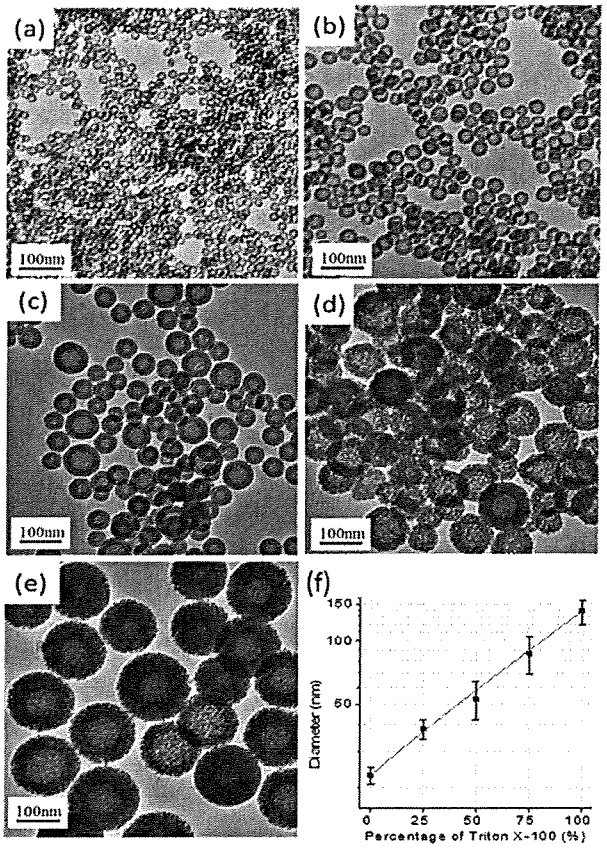

Fig. 9 Representative TEM images of HSNs synthesized with various amounts of (a) 0, (b) 25%, (c) 50%, (d) 75% and (e) 100% Triton X-100 over CA-520. (f) Correlation of Triton X-100 molar ratio (%) to HSNs' diameters (in log scale).

polydispersity in diameters when the percentage of Triton X-100 in the system was larger than 50%. The microemulsion behaviors in the mixing system do not follow a single size distribution, and the DLS analysis for the microemulsion in Fig. S7† indicates bimodal size distributions (5 nm and at 21 nm) of the water droplets before the addition of TEOS or APTS. But the final size distribution is still weakly bimodal. For example, when the percentage of Triton X-100 was 75%, the final SSN sizes were also redistributed into a bimodal profile having two centers at around 60 and 90 nm (Fig. S7† inset). This clearly suggests that in this case, the size-focusing effect is not strong enough to lead to monodisperse distribution of the size of the final SSNs.

4. Discussion

In this section, we discuss the physical chemistry behind the growth process and the control of HSN particle size in a reverse microemulsion. The chemical reactions involved in silica formation from TEOS, hydrolysis (eqn (1)) and condensation (eqn (2) and (3)), as catalyzed by the highly alkaline ammonia solution, are as follows:

$$\equiv\text{Si–OEt} + \text{H}_2\text{O} \rightarrow \equiv\text{Si–OH} + \text{EtOH} \quad (1)$$

$$\equiv\text{Si–OH} + \text{EtO–Si}\equiv \rightarrow \equiv\text{Si–O–Si}\equiv + \text{EtOH} \quad (2)$$

$$\equiv\text{Si–OH} + \text{HO–Si}\equiv \rightarrow \equiv\text{Si–O–Si}\equiv + \text{H}_2\text{O} \quad (3)$$

The net reaction is:

$$(\text{EtO})_4\text{Si} + 2\text{H}_2\text{O} \rightarrow \text{SiO}_2 + 4\text{ROH} \quad (4)$$

As the reactions proceed, TEOS consumes water and produces EtOH while forming silanol and siloxane bonds. This makes the silicate species (oligomers) gradually move from the continuous phase to the water droplets, where further condensation occurs. Meanwhile, the water droplet provides an environment similar to Stöber synthesis with a mixture of ammonia, water and ethanol solution. The droplet size grows initially as hydrolyzed silicates and APTS move into the water droplets. In fact, this can be regarded as a Stöber-like reaction occurring in a soft-confined nanoreactor space. Then, the silica nanoparticles grow by coalescence as silica condensation reaction takes over as the driving force for growth.

4.1 Evolution of silica nanoparticles within the reverse microemulsion

Here, the role of microemulsion in the synthesis of SSNs is examined to compare to the classical Stöber process. We focus on the evolution of size and SLD of the silica nanoparticles as depicted in Fig. 4c. In principle, there are three growth modes for nanoparticles:[54] classic (LaMer) nucleation and growth, aggregative growth, and Ostwald ripening. In our system, the microemulsion droplet-compartmentalized silicate species made the aggregation *via* inter-micellar contacts much slower compared to the corresponding Stöber process in homogeneous solution. The slowed-down kinetics allows us to observe *in situ* the different stages in growth. Also, in microemulsion synthesis, the mass transfer of silica precursors *via* shrinkage and dissolution into the oil phase is not effective. The Ostwald ripening process, in our case, is not an important pathway in the microemulsion synthesis, at least initially.

Next, we examine the time evolution of diameter and SLD as presented in Fig. 4c. In the beginning, one sees stage 1 at the first half hour, when neither the SLD nor the size changed much. This is the induction period for nucleation.[55] Hydrolysis reaction and solubilization occur, but little silica condensation has occurred yet. We note here that previous time-evolution studies of the Stöber process[56] did not identify any induction period because it was much faster in homogeneous solution compared to our reverse microemulsion system. In stage 2 (~30 to 100 min), one observes a rapid increase of SLD (Fig. 4a), which we interpret as the nucleation burst period. A LaMer nucleation/growth process and critical size aggregation result in a bimodal size distribution. In the same period, the mean particle diameter grows to about 18 nm but with a very large variance in size distribution at the end of the nucleation

 This journal is © The Royal Society of Chemistry 2015

Published on 22 April 2015. Downloaded by National Tsing Hua University on 22/06/2015 03:13:24.

period. This is reasonable, since each particle will immediately grow after nucleation, and this leads to big differences in sizes between particles that were nucleated at different times of the nucleation burst period. At the end of the burst period, the size distribution is the broadest, as we clearly see at 100 min. Between 100 and 400 min (stage 3), the nucleation stops, and growth by diffusion/coalescence dominates. In the log–log plot of Fig. 4c, one sees a time dependence $\sim t^{1/2}$ (actual fit is $t^{0.48}$), which is characteristic of the classical Lifschitz–Slyozov (LS) for interface kinetic-limited growth.[57] A super-critical silica particle grows by incorporating the silicate species in other reverse micelles (moving diffusively) after collision and fusion. In the final stage (4), the time evolution of diameter slows down to a power law of $t^{0.21}$. The particle size slowly reaches a limiting value of ~37 nm. Because of this slow-down, the size distribution is self-focusing and becomes narrower. This makes the reverse microemulsion method advantageous in size uniformity. According to LS theory, if the growth is changed to diffusion-limited, the time evolution of the diameter would be $t^{1/3}$ under unchanging concentration at infinite distance. Our observation of a slower growth law of $t^{0.21}$ may be due to the additional effect of a decreasing population of reverse micelles in solution.

Recently, in a detailed *in situ* SAXS study of Stöber synthesis of silica nanoparticles, Tobler *et al.* found a 3-stage growth process:[58] (1) nucleation of silica nanoparticles, (2) surface-controlled particle growth and (3) Ostwald ripening (OR) and particle aggregation. In our synthesis of silica nanoparticles, we found a first stage of induction period for the nucleation event and surface-limited particle growth by fusion of small reverse micelles. The surface-controlled growth by incorporation of silicate-containing reverse micelles was evidenced by the $t^{1/2}$ dependence profile in our stage (2) and (3). However, unlike most solution syntheses of nanoparticles, the final stage of decreasing variance in size distribution of our stage (4) makes the OR mechanism unlikely. Because of the compartmental effect of reverse micelles, Ostwald Ripening and aggregation are much reduced. Instead, we observed a final slow-down stage (4) allowing a self-focusing effect on the size distribution of silica nanoparticles produced.

4.2 The effects of changing continuum phase and interface composition

The final diameters of the silica nanoparticles are determined by coalescence kinetics of critical-sized nanoparticles. We have seen that among the four stages of time evolution, the diffusive coalescence of micellar droplets (red line in Fig. 4c) dominates the growth process. Thus, we made changes in the synthesis compositions in order to control the coalescence kinetics. Here we report three synthesis parameters on growing silica nanoparticles for different sizes: continuous phases, co-solvent amounts and surfactant mixture ratios.

In a reverse microemulsion system, the continuous phase (oil) interacts with hydrophobic parts of the surfactants, resulting in stable initial reverse micelles with well-defined sizes. In our microemulsion system, the polymeric surfactants wedge the micelles to lower the curvature. Thus, we examine the spontaneous curvature of the o/w interface when the solvent is varied. In water/oil microemulsion, it has been reported that the radius of spontaneous curvature decreases as the chain length of oil decreases.[59] Indeed, we have measured by dynamic light scattering that the hydrodynamic diameter of the w/o droplet decreases as the chain length becomes shorter, from 5.5 nm for *n*-hexane to 16 nm for *n*-dodecane [see Fig. S5†]. The solvation of the hydrophobic polymeric chain of the surfactant CA-520 by the alkane solvent determines its effective size. A good solvent, such as hexane or cyclohexane, would swell the hydrophobic tails of the polymeric surfactant and give higher curvature for the reverse micelle droplet. In contrast, a poor solvent, such as dodecane with a long alkyl chain, would result in de-solvation and shrinking of the hydrophobic tails. It then gives a lower curvature of the droplet.

When two droplets in a reverse microemulsion collide, they may fuse partially to establish a fluid bridge and exchange contents, and then separate. This coalescence is important when nucleated silica grows inside the droplet. In addition to the attractive interaction due to dispersion force, the short-range, repulsive barrier to fusion is determined by the entropic force between interpenetrating polymer chains. An expanded polymeric configuration in good solvent would suffer more entropy loss when chains encounter each other upon the collision of two interfaces, thus becoming more resistant to fusion.[60] This, then, would give a stronger entropic repulsion between two approaching micelles, which protects the interface from fusion and coalescence. The result is a smaller silica nanoparticle when a good solvent is used as the continuous phase in w/o microemulsion. In Scheme 2, we depict the molecular interactions involved in the coalescence process. The repulsive interaction between the reverse micelles, which gives rise to the energy barrier against coalescence, is entropic in origin. This explains the size trend for different alkane chain lengths in Fig. 7e.

A second factor determining the energy barrier of droplet fusion is the energy spent on forming Gaussian curvatures, *e.g.* saddle-shaped curvature. Here, the magnitude of saddle splay modulus κ' determines the corresponding energy.[61] If κ' is positive and large, the saddle-like surfaces are favored with respect to planar. It has been long known that adding a medium-chain alcohol (such as hexanol) to a surfactant film normally increases the film flexibility for forming saddle-like shaped film.[61,62] The presence of the cosurfactant hexanol decreases the strength of the surfactant film and thus increases the fusion dynamics of micelles. This qualitative trend explains the results of increasing size with hexanol amount in Fig. 8e.

A third, though minor, factor affecting the size of HSNs would be the partition equilibrium of hexanol between oil and micellar phases. Although the partition of hexanol in micellar phase is favored, the large volume of the oil phase makes the dissolution of hexanol in oil significant, which decreases slowly with the chain length of alkanes.[63] So in heavier alkanes, there is more hexanol in the oil–water interface.

Published on 22 April 2015. Downloaded by National Tsing Hua University on 22/06/2015 03:13:24.

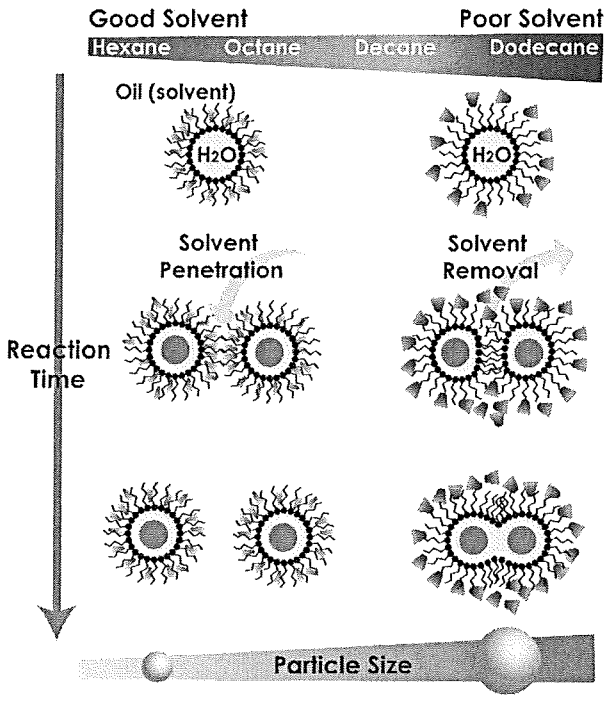

Scheme 2 Solvent-initiated fusion pathways for silica nanoparticle formation. The fusion tendency of droplets in w/o microemulsion is primarily determined by solvent compatibility with the hydrophobic chain as varied in the chain length of the continuous phase (oil).

According to Fig. 9, this effect also tends to make the size of HSNs bigger for the higher alkanes. But this effect is relatively minor compared to the previous ones.

4.3 Why hollow structures are formed

We now discuss the formation of hollow silica nanoparticles after repeated washing SSNs with warm water. Several etching methods have been developed to create internal voids or enlarged pores for incompletely condensed silica nanoparticles. In most literature reports, the methods used for etching of silica are alkaline-based. However, for very small silica nanoparticles, the alkaline-based etching method has been difficult to control. One needs an etching method that is mild and controllable. Yin and coworkers have recently reported warm water as etchant for making permeable silica nanoshells by surface-protected etching.[64] This process is particularly useful for treating small silica nanoparticles. It is expected that the etching efficiency is directly related to the degree of condensation of the silica network.

In our microemulsion-based synthesis, several factors lead to incomplete condensation of silica in the core region of the silica nanoparticle. First, the PEO group in the polymeric surfactants stabilizes silica condensation in the interfacial region. Previously, Yin and coworkers[65] have used poly(vinyl pyrrolidone) (PVP) to stabilize the silica network structure in a "surface-protected etching" approach in making silica nanoshells. Either PVP or PEO can stabilize condensed silanol groups through hydrogen bonding interaction. This makes the shell region more condensed and less prone to etching. Secondly, an ethanol solution of APTS was used in preparing the initial reaction solution, which means that the continuous alkane phase is already saturated with ethanol in the beginning of synthesis. Thus, the EtOH produced in the hydrolysis (eqn (1)) and condensation (eqn (2)) of TEOS and APTS has to stay inside the water pool. When enough EtOH is produced, it will shift the reactions to the left hand side of eqn (1) and (2), *i.e.*, less condensation of silicates. Thirdly, the use of APTS would lead to less silica condensation because it has one less condensable alkoxyl group. However, from our leaching study, we found to our initial surprise that APTS preferentially stays on the silica nanoparticle upon etching with warm water. This is due to the self-catalysis activity of the $-NH_2$ group in APTS for hydrolysis and condensation reaction (eqn (1) and (2)).[66,67] Thus, APTS becomes more condensed than TEOS in the confined space of the microemulsion. Putting the above three factors together, silica condensation of the silica source TEOS and APTS in the water pool of the reverse microemulsion is less complete in the core region and leads to hollow silica nanospheres after etching with warm water.

5. Conclusion

In situ SAXS allows real-time monitoring of the formation of ammonia-catalyzed silica nanoparticles in cyclohexane w/o microemulsion. Co-condensation of TEOS and APTS during the growth of silica creates an interesting system of partially condensed nanospheres that possess highly negative potentials at pH 7. Etching with warm water of the silica nanoparticles then produces uniform hollow silica nanospheres. The silica nanoparticle diameters can be rationally controlled by changing the oil phases, co-surfactants or mixing surfactant ratios. The diameter tuning range (20–160 nm) allows us to explore the micelle growth pathway *via* aggregation and coalescence, where the evolution of both diameter and SLD values suggest sigmoidal-like growth kinetics. Upon detailed examination of the kinetics with *in situ* SAXS, the evolution of bimodal narrow distributions of the growing nanoparticles and a small, constant-sized water droplet could be followed in the aggregative coarsening behaviors in w/o microemulsion. We identify four stages of evolution: induction, nucleation, diffusional growth and slow down. This study provides detailed knowledge for controlling the size and distribution of the hollow silica nanospheres.

Acknowledgements

We are grateful to the National Synchrotron Radiation Research Center (Hsinchu, Taiwan) for support in SAXS experiments and data analysis, the National Taiwan University and Minister of Science and Technology (NSC-100-2120-M-002-011)

 This journal is © The Royal Society of Chemistry 2015

Published on 22 April 2015. Downloaded by National Tsing Hua University on 22/06/2015 03:13:24.

for financial support, and the Instrument Center of National Taiwan University for assistance in TEM and solid-state NMR experiments.

References

1 J. Lee, J. C. Park and H. Song, *Adv. Mater.*, 2008, **20**, 1523–1528.
2 L. L. Li, F. Q. Tang, H. Y. Liu, T. L. Liu, N. J. Hao, D. Chen, X. Teng and J. Q. He, *ACS Nano*, 2010, **4**, 6874–6882.
3 J. Lian, Y. Xu, M. Lin and Y. T. Chan, *J. Am. Chem. Soc.*, 2012, **134**, 8754–8757.
4 J. Dou and H. C. Zeng, *J. Am. Chem. Soc.*, 2012, **134**, 16235–16246.
5 S. H. Wu, C. T. Tseng, Y. S. Lin, C. H. Lin, Y. Hung and C. Y. Mou, *J. Mater. Chem.*, 2011, **21**, 789–794.
6 C. H. Lin, X. Y. Liu, S. H. Wu, K. H. Liu and C. Y. Mou, *J. Phys. Chem. Lett.*, 2011, **2**, 2984–2988.
7 S. S. Cao, L. Fang, Z. Y. Zhao, Y. Ge, S. Piletsky and A. P. F. Turner, *Adv. Funct. Mater.*, 2013, **23**, 2162–2167.
8 F. P. Chang, Y. Hung, J. H. Chang, C. H. Lin and C. Y. Mou, *ACS Appl. Mater. Interfaces*, 2014, **6**, 6883–6890.
9 Y. S. Lin, S. H. Wu, C. T. Tseng, Y. Hung, C. Chang and C. Y. Mou, *Chem. Commun.*, 2009, 3542–3544.
10 S. Mohapatra, S. R. Rout, R. Narayan and T. K. Maiti, *Dalton Trans.*, 2014, **43**, 15841–15850.
11 M. Chen, L. Wu, S. Zhou and B. You, *Adv. Mater.*, 2006, **18**, 801–806.
12 W. J. Li, X. X. Sha, W. J. Dong and Z. C. Wang, *Chem. Commun.*, 2002, 2434–2435.
13 H. J. Hah, J. S. Kim, B. J. Jeon, S. M. Koo and Y. E. Lee, *Chem. Commun.*, 2003, 1712–1713.
14 H. P. Lin, Y. R. Cheng and C. Y. Mou, *Chem. Mater.*, 1998, **10**, 3772–3776.
15 Y. Q. Yeh, B. C. Chen, H. P. Lin and C. Y. Tang, *Langmuir*, 2006, **22**, 6–9.
16 H. P. Hentze, S. R. Raghavan, C. A. McKelvey and E. W. Kaler, *Langmuir*, 2003, **19**, 1069–1074.
17 J. Yuan, X. T. Bai, M. W. Zhao and L. Q. Zheng, *Langmuir*, 2010, **26**, 11726–11731.
18 P. A. Williamson, P. J. Blower and M. A. Green, *Chem. Commun.*, 2011, **47**, 1568–1570.
19 S. P. Moulik and B. K. Paul, *Adv. Colloid Interface Sci.*, 1998, **78**, 99–195.
20 L. Yang, R. S. Xie, L. Y. Liu, D. Q. Xiao and J. G. Zhu, *J. Phys. Chem. C*, 2011, **115**, 19507–19512.
21 V. Tchakalova, F. Testard, K. Wong, A. Parker, D. Benczedi and T. Zemb, *Colloids Surf., A*, 2008, **331**, 31–39.
22 X. J. Zhao, R. P. Bagwe and W. H. Tan, *Adv. Mater.*, 2004, **16**, 173–176.
23 S. Santra, R. P. Bagwe, D. Dutta, J. T. Stanley, G. A. Walter, W. Tan, B. M. Moudgil and R. A. Mericle, *Adv. Mater.*, 2005, **17**, 2165–2169.
24 F. J. Arriagada and K. Osseo-Asare, *J. Colloid Interface Sci.*, 1999, **211**, 210–220.
25 F. J. Arriagada and K. Osseo-Asare, *Colloids Surf., A*, 1999, **154**, 311–326.
26 H. M. Chen, T. Hu, X. M. Zhang, K. F. Huo, P. K. Chu and J. H. He, *Langmuir*, 2010, **26**, 13556–13563.
27 J. Wang, Z. H. Shah, S. Zhang and R. Lu, *Nanoscale*, 2014, **6**, 4418–4437.
28 J. Eastoe, M. J. Hollamby and L. Hudson, *Adv. Colloid Interface Sci.*, 2006, **128–130**, 5–15.
29 A. K. Ganguli, A. Ganguly and S. Vaidya, *Chem. Soc. Rev.*, 2010, **39**, 474–485.
30 Y. H. Jin, A. Z. Li, S. G. Hazelton, S. Liang, C. L. John, P. D. Selid, D. T. Pierce and J. X. Zhao, *Coord. Chem. Rev.*, 2009, **253**, 2998–3014.
31 J. N. Park, A. J. Forman, W. Tang, J. H. Cheng, Y. S. Hu, H. F. Lin and E. W. McFarland, *Small*, 2008, **4**, 1694–1697.
32 C. W. Lu, Y. Hung, J. K. Hsiao, M. Yao, T. H. Chung, Y. S. Lin, S. H. Wu, S. C. Hsu, H. M. Liu, C. Y. Mou, C. S. Yang, D. M. Huang and Y. C. Chen, *Nano Lett.*, 2007, **7**, 149–154.
33 A. F. Zhang, Y. C. Zhang, N. Xing, K. K. Hou and X. W. Guo, *Chem. Mater.*, 2009, **21**, 4122–4126.
34 S. J. Park, Y. J. Kim and S. J. Park, *Langmuir*, 2008, **24**, 12134–12137.
35 S. Shi, M. Wang, C. Chen, F. Lu, X. Zheng, J. Gao and J. Xu, *RSC Adv.*, 2013, **3**, 1158–1164.
36 F. P. Chang, Y. P. Chen and C. Y. Mou, *Small*, 2014, **10**, 4785–4795.
37 Z. Jin, F. Wang, F. Wang, J. X. Wang, J. C. Yu and J. F. Wang, *Adv. Funct. Mater.*, 2013, **23**, 2137–2144.
38 Z. G. Teng, X. D. Su, Y. Y. Zheng, J. Sun, G. T. Chen, C. C. Tian, J. D. Wang, H. Li, Y. N. Zhao and G. M. Lu, *Chem. Mater.*, 2013, **25**, 98–105.
39 X. L. Fang, Z. H. Liu, M. F. Hsieh, M. Chen, P. X. Liu, C. Chen and N. F. Zheng, *ACS Nano*, 2012, **6**, 4434–4444.
40 Y. H. Jin, S. Lohstreter, D. T. Pierce, J. Parisien, M. Wu, C. Hall and J. X. J. Zhao, *Chem. Mater.*, 2008, **20**, 4411–4419.
41 F. Asaro, A. Benedetti, N. Savko and G. Pellizer, *Langmuir*, 2009, **25**, 3224–3231.
42 P. Riello, M. Mattiazzi, J. S. Pedersen and A. Benedetti, *Langmuir*, 2008, **24**, 5225–5228.
43 F. Asaro, A. Benedetti, I. Freris, P. Riello and N. Savko, *Langmuir*, 2010, **26**, 12917–12925.
44 K. S. Finnie, J. R. Bartlett, C. J. A. Barbe and L. G. Kong, *Langmuir*, 2007, **23**, 3017–3024.
45 D. Langevin, *Annu. Rev. Phys. Chem.*, 1992, **43**, 341–369.
46 A. Gutierrez-Becerra, M. Barcena-Soto, V. Soto, J. Arellano-Ceja, N. Casillas, S. Prevost, L. Noirez, M. Gradzielski and J. I. Escalante, *Nanoscale Res. Lett.*, 2012, **7**, 1–12.
47 P. Podsiadlo, S. G. Kwon, B. Koo, B. Lee, V. B. Prakapenka, P. Dera, K. K. Zhuravlev, G. Krylova and E. V. Shevchenko, *J. Am. Chem. Soc.*, 2013, **135**, 2435–2438.

Published on 22 April 2015. Downloaded by National Tsing Hua University on 22/06/2015 03:13:24.

48 Y. Chen, P. Xu, H. Chen, Y. Li, W. Bu, Z. Shu, Y. Li, J. Zhang, L. Zhang, L. Pan, X. Cui, Z. Hua, J. Wang, L. Zhang and J. Shi, *Adv. Mater.*, 2013, **25**, 3100–3105.
49 R. M. Anisur, J. Shin, H. H. Choi, K. M. Yeo, E. J. Kang and I. S. Lee, *J. Mater. Chem.*, 2010, **20**, 10615–10621.
50 Q. W. Shanshan Li, Z. Qin, Y. Fu and Y. Gu, *Langmuir*, 2015, **31**, 824–832.
51 C.-L. Chang and H. S. Fogler, *Langmuir*, 1997, **13**, 3295–3307.
52 V. F. Sears, *Neutron News*, 1992, **3**, 26–37.
53 C. L. Chang and H. S. Fogler, *AIChE J.*, 1996, **42**, 3153–3163.
54 F. D. Wang, V. N. Richards, S. P. Shields and W. E. Buhro, *Chem. Mater.*, 2014, **26**, 5–21.
55 S. J. D.L. Green, Y.-F. Lam and M. T. Harrisa, *J. Non-Cryst. Solids*, 2003, **315**, 166–179.
56 D. Pontoni, T. Narayanan and A. R. Rennie, *Langmuir*, 2002, **18**, 56–59.
57 I. M. Lifshitz and V. V. Slyozov, *J. Phys. Chem. Solids*, 1961, **19**, 35–50.
58 D. J. Tobler, S. Shaw and L. G. Benning, *Geochim. Cosmochim. Acta*, 2009, **73**, 5377–5393.
59 M. J. Hou and D. O. Shah, *Langmuir*, 1987, **3**, 1086–1096.
60 B. Lemaire, P. Bothorel and D. Roux, *J. Phys. Chem.*, 1983, **87**, 1023–1028.
61 A. Kabalnov, B. Lindman, U. Olsson, L. Piculell, K. Thuresson and H. Wennerström, *Colloid Polym. Sci.*, 1996, **274**, 297–308.
62 P. G. De Gennes and C. Taupin, *J. Phys. Chem.*, 1982, **86**, 2294–2304.
63 R. Aveyard and R. W. Mitchell, *Trans. Faraday Soc.*, 1969, **65**, 2645–2653.
64 Y. X. Hu, Q. Zhang, J. Goebl, T. R. Zhang and Y. D. Yin, *Phys. Chem. Chem. Phys.*, 2010, **12**, 11836–11842.
65 Q. Zhang, T. R. Zhang, J. P. Ge and Y. D. Yin, *Nano Lett.*, 2008, **8**, 2867–2871.
66 I. A. Rahman, M. Jafarzadeh and C. S. Sipaut, *Ceram. Int.*, 2009, **35**, 1883–1888.
67 A. van Blaaderen and A. Vrij, *J. Colloid Interface Sci.*, 1993, **156**, 1–18.

This journal is © The Royal Society of Chemistry 2015